Effect of Stitching on Debonding in Composite Structural Elements

I.S. Raju and E.H. Glaessgen
Analytical and Computational Methods Branch
NASA Langley Research Center, Hampton, VA 23681-0001, U.S.A.

Paper for the
International Conference on Computational Engineering and Science

August 2001

Effect of Stitching on Debonding in Composite Structural Elements

I.S. Raju and E.H. Glaessgen
NASA Langley Research Center
Hampton, VA 23681, U.S.A.

Summary

Stitched multiaxial warp knit materials have been suggested as viable alternatives to laminated prepreg materials for large aircraft structures such as wing skins. Analyses have been developed to quantify the effectiveness of stitching for reducing strain energy release rates in skin-stiffener debond, lap joint and sandwich debond configurations. Strain energy release rates were computed using the virtual crack closure technique. In all configurations, the stitches were shown to significantly reduce the strain energy release rate.

Introduction

Multiaxial warp knit, 2-D braided, 3-D braided and stitched textile material forms have great potential for application to composite aircraft structures and are shown in Figure 1. The advantages and limitations of each of the material forms are presented in [1]. Among the textile material forms that have been developed for aircraft structures, stitched multiaxial warp knit materials have proven to be the most viable for large aircraft structures such as wing skins.

Stitching is expected to suppress the initiation and growth of debonds between the layers of the skin and between the stiffeners and skin. The structural skins are typically made of between two and ten stacks (layers of material) of 0.055 in. thick carbon warp-knit fabric that is layered and stitched with Kevlar yarns. The stiffeners and intercostals are fabricated with a similar number of stacks of stitched fabric and are then stitched to the skin. Once the preform is assembled, resin film infusion (RFI) is used to impregnate the entire structure with epoxy resin [1]. Skin-stiffener interface stresses may be large enough to cause a separation between the skin and stiffening elements resulting in a delamination or debond. The effects of stitching on delamination or debond growth in composites have been examined in [2]. This paper summarizes the results of fracture mechanics analyses of skin-stiffener debond, lap joint and sandwich debond configurations shown in Figure 2. Continuum (2-D and 3-D) and plate finite elements are used to model the configuration and the strain energy release rates are calculated using the virtual crack closure technique (VCCT) to study the effectiveness of stitching. The stitches are modeled as nonlinear spring elements with axial and shear compliances determined by experiment.

Analysis

A typical stitched wing skin configuration with stiffeners and intercostals is shown in Figure 2(a) and a typical stitched sandwich configuration is shown in Figure 2(b). In these configurations, debonds can occur between the stiffener and skin, between the layers of skin, or between the skin and core. Considerable insight into the behavior of complex configurations with debonds can be gained by examining simple configurations such as the skin-stiffener debond, lap joint and sandwich debond configurations shown in Figure 3.

Material and skin thicknesses that are representative of the hybrid IM7/3501-6 and AS4/3501-6 warp-knit fabric stitched composite upper wing skin are considered [1]. The material consists of IM7 yarns in the axial direction (warp direction where warp is also the direction of the load) and AS4 yarns in the off-axis directions. Each stack of material is assumed to be oriented with its primary axis in the x-direction and having a thickness of 0.055 in. The overall density of the fabric expressed in areal weight is 0.577 oz./ft.^{2}, 1.21 oz./ft.^{2} and

0.651 oz./ft.^{2} for the forty-five, zero and ninety degree plies, respectively. The equivalent laminate stacking sequence of each stack of material is $(45/-45/0/90/0/-45/45)_{ns}$ In these analyses, the laminates are assumed to be homogeneous with axial properties determined experimentally and all others estimated using the equivalent stacking sequence and classical lamination theory as

E_{11}=11.7 *Msi*	μ_{12}=2.50 *Msi*	υ_{12}=0.40
E_{22}=5.14 *Msi*	μ_{13}=1.77 *Msi*	υ_{13}=0.30
E_{33}=1.79 *Msi*	μ_{23}=0.88 *Msi*	υ_{23}=0.30

where E_{ii}, μ_{ij}, υ_{ij} (i,j=1,2,3) are the Young s moduli, shear moduli, and Poisson s ratio, respectively, and the subscripts 1,2,3 represent the axial (warp), transverse and out-of-plane directions, respectively.

The skin-stiffener debond and lap joint configurations shown in Figures 3(a) and 3(b) were modeled using plate elements (STAGS 480, 9-noded quadratic shear deformable, plate/shell elements). The sandwich debond configuration shown in Figure 3(c) was modeled using plane strain elements (ABAQUS CPE8, 8-noded plane strain (2-D) quadratic element). Note that the offset technique used in plate element modeling [2] is not required for the analyses based on 2-D finite elements. For all three debond configurations, the virtual crack closure technique (VCCT) is used to calculate strain energy release rates, G, using the nodal forces and displacements near the debond front and the debond area created [2].

Compliance curves for both axial and shear behavior of the stitches were developed in reference 3 using flatwise tension and double lap shear tests, respectively. The nonlinear axial and shear stiffness, K_{axial} and K_{shear}, of the spring elements modeling the stitches are extracted from these tests. For the purposes of these analyses, the axial and shear responses of the stitches are assumed to be independent. A piecewise linear representation of this data is used in the finite element model with failure occurring at 58 lb. in tension and 38 lb. in shear [2].

Results and Discussion

All three configurations shown in Figure 3 exhibit both mode I and mode II deformations at the debond front. In the results that follow, both G_I and G_{II} are shown for the skin-stiffener debond and lap joint configurations. However, because of the bimaterial interface between the skin and core, only G_{Total} is shown for the sandwich debond configuration.

The strain energy release rates for the skin-stiffener debond configurations with repeating unit boundary conditions (v=0, θ_x=0 on y=–s_y/2) were determined over a range of debond lengths in Figure 3(a) with skin and flange thickness, t, of 0.220 inches, and a fixed applied load of 100 lb./in. In Figure 4, both the mode I and mode II strain energy release rates, G_I and G_{II}, for the unstitched configurations increase with increasing debond length over a range of debond lengths, $0 \dagger a/t \dagger 9.09$. The increasing strain energy release rates suggest that a condition for unstable debond growth exists in the unstitched configurations.

Stitching has a significant effect on both G_I and G_{II}. The mode-I G-value initially increases with debond length and then begins to decrease after the debond advances past the first stitch (first vertical line in Figure 4), decreasing as additional stitches begin to carry load, eventually reaching values of zero for long debonds (a/t>3.41). These zero values for long debonds correspond to a region of contact immediately behind the debond front that increases with increasing debond length. In contrast, G_{II} is a weaker function of debond length since the shearing displacements are not reduced to zero as the stitches close the debond faces. Rather, the shearing force and displacement are gradually reduced as additional stitches transfer an

increasing fraction of the load. Thus, even though mode-I is driven to zero for $a/t>3.41$ there may be sufficient mode-II present to drive the debond for much longer lengths.

Average debond length vs. load curves were developed from x-ray radiographs of unstitched and stitched 27.0 inch long (L_1) lap joint configurations with a 3.69 inch lap length (L_2). The thickness, t, of 0.110 inches, width, b, of 1.00 inches and stitch spacing, s_x and s_y, of 0.125 inches are used as shown for the stitched configuration in Figure 3(b). In the experiments, debonds grew from only one edge of the unstitched configuration but grew from both edges of the stitched configuration. The strain energy release rates were then determined using the experimental results of debond length vs. load as input parameters in plate element-based finite element analyses.

Since the single lap joint configuration has a finite width, it may exhibit mode I, mode II and mode III strain energy release rates. Also, although a straight debond front is employed to simplify the analyses, a variation in strain energy release rate and stitch force may exist along the length (x-) and across the width (y-) of the lap joint (see Fig. 3(b)). In the results that follow, quantities are given at a y-direction location corresponding to: an interior row of stitches near the centerline of the stitched configuration (stitch row 1); an exterior row of stitches near the edge of the stitched configuration (stitch row 4); and intermediate locations between stitch rows 1 and 2 and stitch rows 3 and 4. These later locations are considered only for the stitched configuration. The y locations denoted as locations A, B, A and B are located at y=0.0625 in., y=0.4375 in., y=0.125 in. and y=0.375 in., respectively, from the configuration centerline (see insert in Figure 5(b)). G-values for both the unstitched and stitched infinite width configurations are also provided. When repeating unit boundary conditions (v=0, θ_x=0 on y=0, $b/2$ in Figure 2b) are applied to the models, the calculated G-values are constant in the y-direction for the unstitched configuration and periodic in the y-direction for the stitched configuration.

Figure 5(a) shows G-values plotted against debond length for the unstitched configuration with a debond at only one end of the single lap joint corresponding to experimentally determined debond lengths. Figure 5(a) shows two nonzero components of G (G_I and G_{II}) near the centerline of the finite width lap joint (Location A) and three nonzero components of G (G_I, G_{II} and G_{III}) near the free edge of the finite width lap joint (Location B). Mode I increases at both locations as the debond grows. Mode II is the largest component of energy release rate and also increases with increasing debond length. Mode III has a value near zero (thus, not shown) in the interior at location A but increases near the free edge (Location B).

The energy release rates computed at locations A and B in the finite width configuration bound the energy release rates computed for the infinite width configuration (shown as G_I and G_{II} in Figure 5(a)). This is a result of the repeating unit boundary conditions in the infinite width models preventing anticlastic deformation while the stress free boundary conditions in the finite width models do not. Additionally, the repeating unit boundary conditions in the infinite width models require mode III to be identically zero along the planes of symmetry.

Figure 5(b) shows the G-values plotted as functions of debond length for the stitched configuration with a debond at each end of the single lap joint corresponding to experimentally determined debond lengths. The computed values of G in Figure 5(b) are at discrete locations between the stitch columns and a smooth curve is drawn between the points. Figure 5(b) shows one nonzero component of G (G_{II}) at locations A and A and two nonzero components of G (G_{II} and G_{III}) at locations B and B. For all debond lengths considered at all locations, the mode I component is nearly zero. As with the unstitched configuration, mode II is the dominant component and is seen to increase with debond length. Although G_{II} increases with increasing debond length, the stitches prevent the debond growth from becoming unstable. As in the

unstitched configuration, mode III has a value near zero in the interior (Locations A and A) but increases near the edge (Locations B and B).

The strain energy release rates for sandwich debond configurations modeled with 2-D plane strain elements were evaluated for debond lengths, a, between 0.250 in. (a/t_f=2.27) and 2.00 in. (a/t_f=18.2) with an applied load, P, of 100 lb. Three core moduli (E_{core}=5220 psi, E_{core}=13340 psi, and $E_{core}=E^{11}_{facesheet}$=11.7 Msi) were considered in this study. As shown in Figure 6(a), the unstitched configurations exhibit increasing G_{Total} with increasing debond length, a, for all three core moduli considered. Also, for all debond lengths larger values of core modulus resulted in decreasing values of G_{Total} as shown in Figure 6(a).

The effect of stitching is shown in Figure 6(b) for configurations with four stitches per inch. The slope of the G_{Total} curve decreases for stitched configurations with foam core and for all debond lengths. The decrease is because of the load transfer of the stitches as shown in Figure 6(b). The slope of the G_{Total} curve does not begin to decrease for the configuration with the stiffest core ($E_{core}=E^{11}_{facesheet}$=11.7 Msi) until the third stitch begins to carry load. The G_{Total} continues to decrease with both the number of loaded stitches and for larger values of debond lengths. The maximum G_{Total} (for the models with the stiffest core) shown in Figure 6(b) is 0.384 in.-lb./in.^{2} at a/t_f=4.54 compared with 18.1 in.-lb./in.^{2} for the corresponding unstitched configuration at a/t_f=18.2. For long debonds (a/t_f>9.09), the strain energy release rate approaches near-zero values in the stitched configurations.

Concluding Remarks

The effects of stitching on strain energy release rates for skin-stiffener, lap joint and sandwich debond configurations were studied using an analysis based on finite elements and the virtual crack closure technique. The skin-stiffener debond and lap joint configurations were modeled using 9-noded quadratic shear deformable plate/shell elements, while the sandwich debond configuration was modeled using 8-noded plane strain quadratic elements. The stitches were modeled as discrete nonlinear spring elements with their compliance determined by experiment.

In all configurations studied, the stitches are very effective in the prevention of debond growth. The computed values of strain energy release rate (G-values) for all the debond configurations studied decrease for longer debond lengths. For the skin-stiffener debond and lap joint configurations, the mode-I G-value (G_{I}) decreases to near zero values when more than three stitches start carrying the load across the debond faces. In contrast, the stitches had less effect on mode II and G_{II} remained significant throughout the range of debond lengths considered. Because of the bimaterial interface between the skin and core, only G_{Total} is computed for the sandwich debond configuration and it also decreases with increasing debond length.

References

1. Dow, M.B. and Dexter, H.B. (1997): Development of Stitched, Braided and Woven Composite Structures in the ACT Program and at Langley Research Center, NASA TP-97-206234.
2. Glaessgen, E.H., Raju, I.S. and Poe, Jr., C.C. (1998): Plate Element-Based Models for Mixed-Mode Debonding of Stitched Stiffened Panels, Fatigue and Fracture Mechanics: 30th Volume, STP 1360, ASTM, pp. 456-472.
3. Adams, D.O. (1997): Stitch Compliance in Delaminated Composites, 29th SAMPE Technical Conference, Orlando, FL, October 28-31.

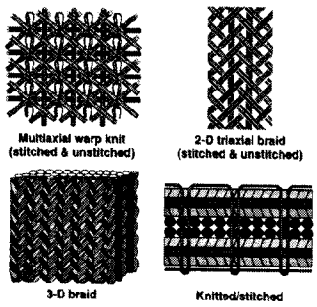

Fig. 1 Textile material forms

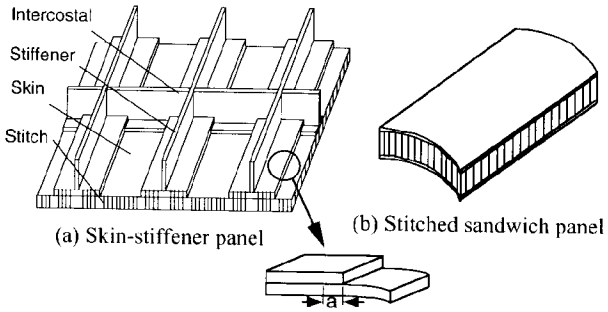

Fig. 2 Stitched composite panels

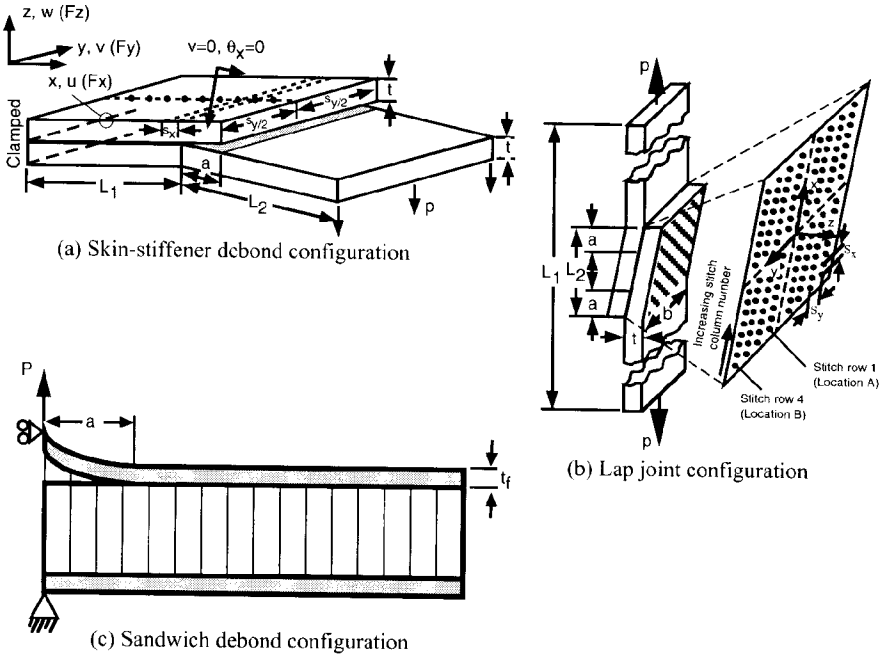

Fig. 3 Configurations considered in the analyses

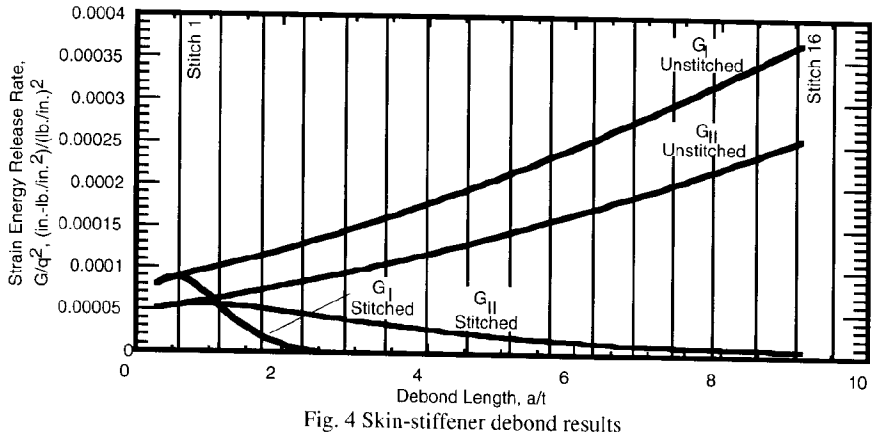

Fig. 4 Skin-stiffener debond results

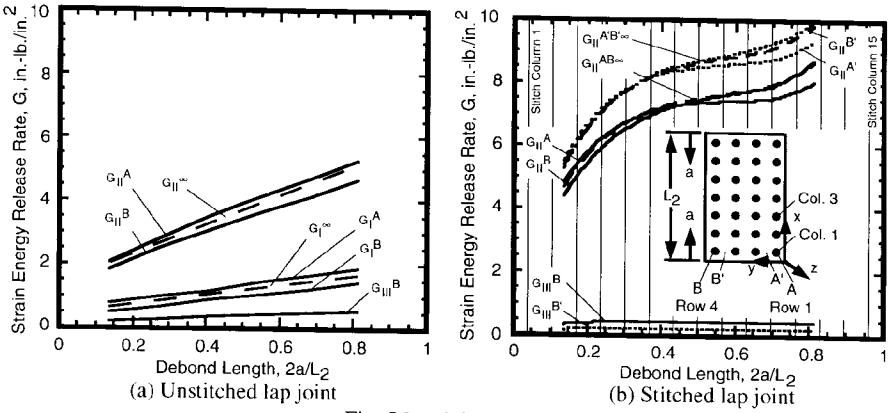

(a) Unstitched lap joint

(b) Stitched lap joint

Fig. 5 Lap joint debond results

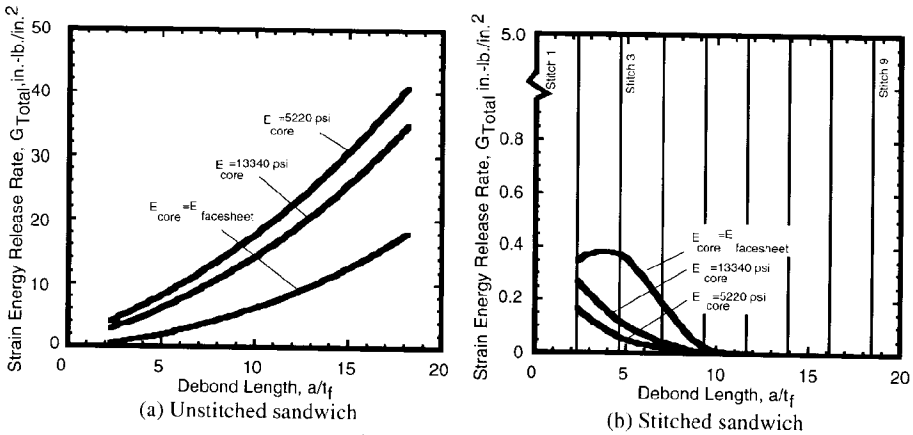

(a) Unstitched sandwich

(b) Stitched sandwich

Fig. 6 Sandwich debond results